Non–diffracting integer and half–integer carpet beams obtained by even–type sinusoidal amplitude radial gratings

Yefeng Liu (刘叶枫), Huiqing Li (黎慧青), Rijian Chen (陈日坚), Changjiang Fan (范长江), Yile Shi (施逸乐), AND Zhijun Ren (任志君)*

Key Laboratory of Optical Information Detecting and Display Technology, Zhejiang Normal University, Jinhua, Zhejiang, 321004, China

**Corresponding author: renzhijun@zjnu.cn*

Received Month X, XXXX; accepted Month X, XXXX; posted online Month X, XXXX

In this work, we introduced a kind of new structured radial grating, which is named as even–type sinusoidal amplitude radial (ETASR) gratings. Based on diffraction theory and the principle of stationary phase, a comprehensive theoretical investigation on the diffraction patterns of ETASR gratings was conducted. Theoretical results show that novel carpet beams with beautiful optical structure and distinctive characteristics have been constructed on the basics of ETASR grating. Their diffraction patterns are independent of propagation distance, that is, the new carpet beams have diffraction–free propagating characteristics. The non–diffracting carpet beams are divided into two types by beam characteristic: non–diffracting integer order and half–integer order carpet beams. Subsequently, we experimentally generate these carpet beams by using ETASR grating. Finally, their particularly interesting optical morphology and features are explored through the numerical stimulation and experiment.

Keywords*:* even–type sinusoidal amplitude radial gratings; principle of stationary phase; non–diffracting integer carpet beams; non–diffracting half–integer carpet beams

DOI: 10.3788/COLXXXXXX.XXXXXX.

1. Introduction

As one of the most important optical elements, gratings with periodic structures have been widely used in many application fields, such as spectral analysis, laser tuning, optical display, optical sensing, and optical storage. In nature, a grating is an optical diffractive element. When beams pass though different diffraction gratings, remarkable and intriguing diffractive behavior can be observed. Talbot self–imaging effects can be regarded as diffraction phenomena at the near–field of a periodic grating [1-3]. Referring the principle of the Talbot effect, Rasouli et al. studied the near–field and far–field propagation behavior of radial periodic gratings with two–dimensional periodic structures, and constructed and generated several kinds of carpet beams [1,2]. Subsequently, various carpet beams with special intensity distributions, even carpet beams with tunable two–dimensional optical lattice structures, have been generated by modulating beams with different phase and amplitude gratings [4-9]. Since the inception of carpet beams, they have inspired numerous applications and intriguing concepts owing to their intricate optical structures and distinctive characteristics. For example, carpet beams have been used in optical tweezers for multiple optical trapping (i.e. multiple trapping of particles over an annular array) [9,10], optical communication [11], indoor optical communication systems [7], optical communication in an underwater medium [12], and production of multiple filament plasma channels [4]. Indeed, carpet beam generation and application have generated considerable experimental and theoretical interest.

Despite that classical carpet beams with different optical structures have been used in some research fields, the above–mentioned carpet beams are not non–diffracting beams. The term "non–diffracting beam" was first introduced to designate zero–order Bessel beams [13]. In the past few decades, rapid progress in the generation and use of various types of non–diffracting beams has been achieved. In some fields, non–diffracting beams play essential roles, even fundamentally changing the working paradigms of some scientific instruments. For example, non–diffracting Bessel beams have been used in optical tweezer [14], super–resolution imaging [15], light sheet microscopy [16], and space–division–multiplexing optical communication systems [17]. Non–diffracting airy beams are used in micrometer–sized "snowblower," [18] optical coherence tomography [19], and curved plasma channel production [20]. Non–diffracting Lommel beams are used in optical wireless communication [21], and Non–diffracting parabolic beams are used as optical tweezers for manipulating the dielectric particles [22]. Many non–diffracting array beams are used in the generation of optical lattices [23-26], ultracold atom trapping [27], and three–dimensional microstructure design [28].

It is readily known that the special beams with non–diffracting propagation characteristics can play a more unique role in optical application field comparing with other ordinary beams. However, the classical carpet beams are not entirely non–diffracting beams. The optical field distribution of classical carpet beams slowly expands during propagation, although the optical structures of classical carpet beams are not altered during propagation. In 2022, Gong et al. explored non–diffracting petal–like beams, which is one of carpet beams [29,30]. The transition of carpet beams from structure–invariant beams (not non–diffracting beams) to non–diffracting beams (of course being structure–invariant beams), is an especially critical progress development [12].

Given that gratings with different structures can generate varying diffraction patterns, we designed a novel type of grating named even–type amplitude sinusoidal amplitude radial (ETASR) grating, which is a kind of amplitude radial grating with an absolute sinusoidal profile. Using the designed ETASR gratings, we theoretically constructed new carpet beams with non–diffracting characteristics based on the principle of stationary phase. To substantiate our findings, we generated non–diffracting carpet beams. This research offers a novel type of carpet beam, especially for the non–diffracting carpet beam family, while providing theoretical insights into its potential applications to some research fields.

2. Theory

In this study, we focused on the creation and exploration of a novel and special carpet beams by designing radial gratings. The diffraction theory of designed grating can be researched from the Fresnel–Kirchhoff's diffraction integral in cylindrical coordinates:

$$U_0(\rho,\theta,z)=\frac{(-i)}{\lambda z}\exp(ikz) \times\int_0^{\infty}\int_0^{2\pi}U_0(r,\varphi)\times\exp\left[\frac{ik}{2z}(r^2+\rho^2)\right]\times\exp[-\frac{ik}{z}\rho r\cos(\varphi-\theta)]r\mathrm{d}r\mathrm{d}\varphi, \tag{1}$$

where λ is the wavelength of the beam, $k=2\pi/\lambda$ is the wavenumber. $U_0(r, \varphi)$ is the complex amplitude distribution of the initial light field (z=0) modulated by mask, r and φ are the radial and azimuth coordinate of the initial field source, respectively, U_0 (ρ, θ, z) is the complex amplitude distribution at the transmission distance z from mask, and ρ and θ are the radial and azimuth coordinate of the observed plane, respectively.

To construct non–diffracting carpet beams with the newly designed gratings, we used the principle of stationary phase. Hence, the axicon phase was necessary in our scheme. The collimated parallel light enters the amplitude mask and axicon successively, and hence the initial light field can be written as:

$$U_0(r,\varphi)=A(\varphi)\exp\left[-ikT(r)\right], \tag{2}$$

where $T(r)$ is phase transform function of the axicon. The radial phase distribution of axicon is [31].

$$T(r)=\begin{cases}(n_0-1)\theta_0 r, & r\le R,\\ 0, & r>R,\end{cases} \tag{3}$$

where n_0 is the refractive index of the axicon. θ_0 is the base angle of the axion, which is usually a small angle, and R is an aperture radius of the entrance pupil of the axicon. In Eq. (2), $A(\varphi)$ is the amplitude transmittance function of the grating. In our scheme, to construct new carpet beams, we introduced even–type amplitude sinusoidal radial gratings. Its transformation function $A(\varphi)$ can be written as:

$$A(\varphi)=\left|\sin(q\varphi)\right|, \tag{4}$$

where q determines the number of gratings' spokes.

Based on mathematical expansion, Eq. (4) can be rewritten as follows:

$$\left|\sin(q\varphi)\right|=\frac{2}{\pi}-\frac{4}{\pi}\sum_{n=-\infty}^{+\infty}\frac{\cos(2nq\varphi)}{(2n-1)(2n+1)}. \tag{5}$$

By using Euler formula $\cos(x)=\frac{e^{ix}+e^{-ix}}{2}$, Eq. (5) can be transformed into the following form:

$$\left|\sin(q\varphi)\right|=\frac{2}{\pi}-\frac{2}{\pi}\sum_{n=-\infty}^{+\infty}\frac{\exp(-2inq\varphi)+\exp(2inq\varphi)}{(2n-1)(2n+1)}. \tag{6}$$

By substituting Eqs. (6) and (4) into Eq. (2) and then substituting the results into Eq. (1), the following expression was obtained:

$$U_0(\rho,\theta,z)=-\frac{i}{\lambda z}\exp(ikz)\frac{2}{\pi}\int_0^{\infty}\int_0^{2\pi}\sum_{n=-\infty}^{+\infty}[1-\frac{\exp(-2inq\varphi)+\exp(2inq\varphi)}{(2n-1)(2n+1)}] \times\exp\left[\frac{ik}{2z}(r^2+\rho^2)\right]\exp\left[-ik(n_0-1)\theta_0 r\right] \times\exp\left[-\frac{ik}{z}\rho r\cos(\varphi-\theta)\right]r\mathrm{d}r\mathrm{d}\varphi. \tag{7}$$

For convenience of mathematically writing, unnecessary terms before integral symbol, which does not affect the distribution of light intensity, were omitted. Moreover, complex amplitude distribution U_0 given in Eq. (7) can be split into three separate equations: U_1, U_2 and U_3:

$$U_0(\rho,\theta,z)=U_1(\rho,\theta,z)+U_2(\rho,\theta,z)+U_3(\rho,\theta,z), \tag{8}$$

where

$$U_1(\rho,\theta,z)=\int_0^{\infty}\int_0^{2\pi}\sum_{n=-\infty}^{+\infty}\frac{\exp(-2inq\varphi)}{(2n-1)(2n+1)}\exp\left[\frac{ik}{2z}(r^2+\rho^2)\right] \times\exp\left[-ik(n_0-1)\theta_0 r\right] \times\exp\left[-\frac{ik}{z}\rho r\cos(\varphi-\theta)\right]r\mathrm{d}r\mathrm{d}\varphi, \tag{9.1}$$

$$U_2(\rho,\theta,z)=\int_0^{\infty}\int_0^{2\pi}\sum_{n=-\infty}^{+\infty}\frac{\exp(2inq\varphi)}{(2n-1)(2n+1)}\exp\left[\frac{ik}{2z}\left(r^2+\rho^2\right)\right] \times\exp\left[-ik(n_0-1)\theta_0 r\right] \times\exp\left[-\frac{ik}{z}\rho r\cos(\varphi-\theta)\right]r\mathrm{d}r\mathrm{d}\varphi, \tag{9.2}$$

and

$$U_3(\rho,\theta,z)=\int_0^{\infty}\int_0^{2\pi}\exp\left[\frac{ik}{2z}\left(r^2+\rho^2\right)\right]\times\exp\left[-ik(n_0-1)\theta_0 r\right]. \times\exp\left[-\frac{ik}{z}\rho r\cos(\varphi-\theta)\right]r\mathrm{d}r\mathrm{d}\varphi. \tag{9.3}$$

Here, we mainly derived Eq. (9.1). Given that the analytic solution of Eq. (9.1) can be extended to Eq. (9.2) given that the two equations have similar mathematical forms. We derived Eq. (9.3) by using the Bessel function.

To derive Eq. (9.1), we used the following Jacobi–Anger expansion [32]:

$$\exp(iz\cos\theta)=\sum_{m=-\infty}^{+\infty}(i)^m J_m(z)\exp(im\theta), \tag{10}$$

where J_m is the m–th order Bessel function of the first kind. From Eq. (10), the following expression was obtained:

$$\int_0^{2\pi}\exp\left[-\frac{ik}{z}\rho r\cos(\varphi-\theta)\right]\mathrm{d}\varphi =\sum_{m=-\infty}^{+\infty}(-i)^m J_m\left(\frac{k}{z}\rho r\right)\int_0^{2\pi}\exp\left[-im(\varphi-\theta)\right]\mathrm{d}\varphi. \tag{11}$$

By substituting Eq. (11) into Eq. (9.1), there is:

$$U_1(\rho,\theta,z)=\sum_{n=-\infty}^{+\infty}\sum_{m=-\infty}^{+\infty}\frac{2i}{\lambda z\pi}\exp(ikz) \times\exp\left(\frac{ik}{2z}\rho^2\right)\int_0^{\infty}(-i)^m J_m\left(\frac{k}{z}\rho r\right) \times\exp\left\{ik\left[\frac{r^2}{2z}-(n_0-1)\theta_0 r\right]\right\}r\mathrm{d}r \times\exp(im\theta)\int_0^{2\pi}\exp\left[i(2nq-m)\varphi\right]\mathrm{d}\varphi. \tag{12}$$

To solve Eq. (12), the following equation was used:

$$\int_0^{2\pi}\exp\left[i(m-q)\varphi\right]\mathrm{d}\varphi=2\pi\delta_{m,q}, \tag{13}$$

where $\delta_{m,q}$ is the Kroneck function. In the Kroneck function, the function has a value of 2π when $m=q$, and the function has value of 0 when $m\neq q$. Thus Eq. (12) was written as:

$$U_1(\rho,\theta,z)=\sum_{n=-\infty}^{+\infty}\frac{2ik}{z\pi}\exp(ikz)\exp\left(\frac{ik}{2z}\rho^2\right)\exp(i2nq\theta) \times\int_0^{\infty}(-i)^{2nq}J_{2nq}\left(\frac{k}{z}\rho r\right)\times\exp\left[ik\left(\frac{r^2}{2z}-(n_0-1)\theta_0 r\right)\right]r\mathrm{d}r. \tag{14}$$

In mathematics, Eq. (14) is a complex integral expression. Hence obtaining its analytic solution by directly solving the integral equation is difficult. In the near–field diffraction, the principle of stationary phase approximation is an important method for simplifying the oscillatory integral with the from $\int g(r)\exp[ikf(r)]\mathrm{d}r$ when $k\rightarrow\infty$ [33]. To solve complex Fresnel integral equation by using stationary phase method, one can set $f(r)=r^2/(2z)-(n_0-1)\theta_0 r$ and $g(r)=J_{2nq}(k\rho r/z)r$ for Eq. (14). By taking the derivative $f(r)$, the stationary phase point can be obtained when $r_0=(n_0-1)\theta_0 z$. Given the size of the entrance pupil of axicon, $r=r_0\in(0, R)$. We obtained the maximum non–diffraction distance $z_{max}=R/[(n_0-1)\theta_0]$ of non–diffracting carpet beams. Hence, the analysis result of Eq. (14) at $0<z<z_{max}$ is:

$$U_1(\rho,\theta,z)=\frac{2ik}{\pi}\sqrt{\lambda z}\exp(ikz)\exp\left(\frac{ik}{2z}\rho^2\right) \times\exp\left[i\left(-\frac{k\left[(n_0-1)\theta_0\right]^2 z}{2}+0.25\pi\right)\right] \times\sum_{n=-\infty}^{+\infty}(-i)^{2nq}\exp(2inq\theta)J_{2nq}(k_r\rho). \tag{15}$$

Using the similar method, the analytical result of Eq. (9.2) and (9.3) can be obtained:

$$U_2(\rho,\theta,z)=\frac{2ik}{\pi}\sqrt{\lambda z}\exp(ikz)\exp\left(\frac{ik}{2z}\rho^2\right) \times\exp\left[i\left(-\frac{k\left[(n_0-1)\theta_0\right]^2 z}{2}+0.25\pi\right)\right] \times\sum_{n=-\infty}^{+\infty}(-i)^{-2nq}\exp(-2inq\theta)J_{-2nq}(k_r\rho), \tag{16}$$

$$U_3(\rho,\theta,z)=\frac{2ik}{\pi}\sqrt{\lambda z}\exp(ikz)\exp\left(\frac{ik}{2z}\rho^2\right) \times J_0(k_r\rho)\exp\left[i\left(-\frac{k\left[(n_0-1)\theta_0\right]^2 z}{2}+0.25\pi\right)\right]. \tag{17}$$

By bringing Eqs. (15), (16), and (17) into Eq. (8), we obtained the final expression of a kind of new carpet beam by using the amplitude modulation element of ETASR gratings.

$$U_0(\rho,\theta,z)=\frac{2ik}{\pi}\sqrt{\lambda z}\exp(ikz)\exp\left(\frac{ik}{2z}\rho^2\right)$$
$$\times\exp\left(i\left\{-\frac{k\left[(n_0-1)\theta_0\right]^2 z}{2}+0.25\pi\right\}\right) \tag{18}$$
$$\times\sum_{n=-\infty}^{+\infty}[(-i)^{2nq}\exp(-2inq\theta)J_{-2nq}(k_r\rho)$$
$$+(-i)^{2nq}\exp(2inq\theta)J_{2nq}(k_r\rho)+J_0(k_r\rho)].$$

Equation (18) is the main analytical result that describes the diffracted amplitude of the ETSAR gratings. One can obtained the main physical insight from this above mathematical expression. From the sum expression, we know that all Bessel functions have the same transverse wave number. Moreover, the radial wave number of each order Bessel function is independent of the propagation distance z. It is readily known that the superposition of non–diffracting beams with the same transverse wave number is still a non–diffracting beam. The intensity distribution of the kind of the newly constructed carpet beams by using ETASR gratings is

$$I(\rho,\theta,z)=U_0(\rho,\theta,z)U_0^*(\rho,\theta,z), \tag{19}$$

where * denotes a complex conjugate. From the sum expression given in Eq. (18), the main feature of these diffraction patterns is that the radial wavenumber of all Bessel function is independent of the propagating distance z. In addition, all Bessel functions have the same transverse wavenumber, indicating that these kinds of carpet beams are novel non–diffracting beams. In addition, Eq. (18) shows that $U_0(\rho, \theta, z)$ can be calculated when $2nq$ is an integer, that is, $2q$ must be an integer. When $2q$ is an even number, q is an integer number. When $2q$ is an odd number, q is a half–integer. Hence these carpet beams can be divided into two categories according to whether q is an integer or a half–integer : integer order and half–integer order carpet beams.

3. Simulation and experiments

To validate the correctness of the mathematical derivation, we numerically simulated and experimentally investigated the carpet beams. We selected multiple samples to showcase this type carpet, starting from different ETASR gratings. Referring to Eq. (4), we typically drew ETASR gratings with different q value (Fig. 1). In Fig. 1, $2q$ determines the number of spokes of a radial grating. According to the number of grating spokes, they were named radial even– or odd–type grating.

From Eq. (19), the corresponding intensity and phase distribution of carpet beams were simulated with the same parameters as Fig. 1, as shown in Fig. 2. The carpet beams given in Fig. 2 can be generated using ETASR gratings given in Fig. 1. Apparently, each ETASR grating is accompanied by its own characteristic diffraction pattern. The main characteristic of all diffraction carpet patterns was that they are shape invariant during propagation. The structure of a carpet beam strongly depends on the number of grating spokes ($2q$). The main characteristic of the integer order and half–integer order carpet beams is that the central part of the beam is a main lobe, in which the intensity becomes predominant. The main lobe is axial caustic owing to the interference of the intersecting portions of the optical wave. Moreover, the horizontal and vertical symmetry of both types of carpet beams is observed.

The beam structures of the integer order or half–integer order carpet beams were explored in detail. For integer order carpet beams, the transverse plane of the diffraction patterns of the gratings can be divided into three distinct areas. The central area is a concentric ring surrounding the main lobe. The area of the concentric ring increases with parameter q. On the periphery of the concentric ring (middle area of beams), a radial divergent toroidal lattice structure forms. In the outward area, another divergent toroidal lattice is present. The radial row of lattice in the outward area is situated at the intermediate area between two adjacent radial lattices of middle area. As for half–integer order carpet beams, the optical structure of the central area is similar to the central area of the integer order carpet beams, but they differ in toroidal lattice structure. On the periphery of a concentric ring, half–integer order carpet beams only exist an area with a radial divergent ring lattice structure. In the central areas of both types of carpet beams, the phase of each concentric ring along angular direction is invariant constant.

The anomalous axial phase behavior of optical beams has been drawing attention since Gouy's discovery in 1890 [34]and is often referred to as the Gouy phase or phase anomaly. This peculiar phase behavior is worth studying because it plays an essential role in some physical problems and applications area [8,35]. A similar phase anomalous behavior can be observed in the integer and half–integer carpet beams (Fig.3). Except the central area, the general trend of the phase change along the r–axis and ρ–axis is the same for integer order and half–integer order carpet beams, and the phase jumps are close to 2π, which are also integer multiples of $\pi/2$ [8,35]. The existence of abrupt phase changes provides an amazing behavior for the corresponding intensity distribution of light field during propagation.

Moreover, a detailed study of the phase anomaly of the light field in radial direction has been conducted, discussing the anomaly in integer order and half–integer order carpet beams. For integer order carpet beams, all phases in the area in the concentric ring and divergent toroidal lattice exhibit anomalous behavior, as shown in Fig. 3 (a). In the central and peripheral areas, the phase of the concentric ring periodically changes, and the value of this phase change is close to π. However, a phase jump at the junction of the two adjacent areas is close to 2π. Similar to the phase of the integer order carpet beams, the phase of the concentric ring in the radial direction

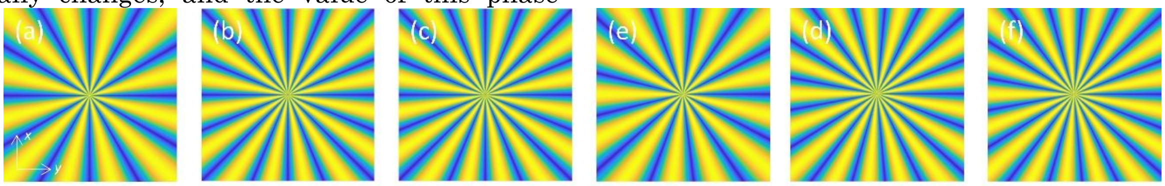

Fig. 1 ETASR gratings with different q values. (a) q = 6; (b) q = 8; (c) q = 10; (d) q = 6.5; (e) q = 8.5; (f) q = 10.5

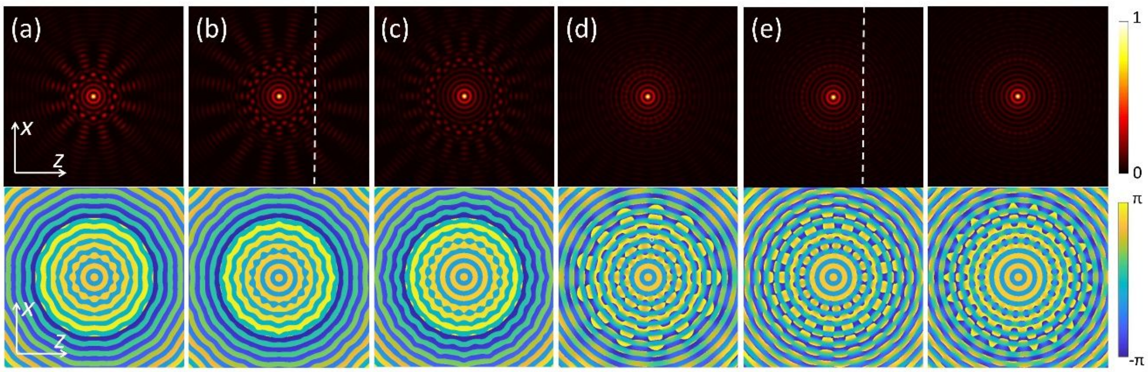

Fig. 2 The simulations graph of carpet beams. First row: the intensity pattern. Second row: the phase pattern. The parameter corresponding to Fig. 1.

in the half–integer order carpet beams' central areas periodically change, as shown in Fig. 3 (b). In the whole peripheral area, the phase change of the half–integer order carpet beams are greater than that of the integer order carpet beams in the radial direction. Moreover, the phase shift of the half–integer order carpet beams is clearer than that of the integer order carpet beams, which may originate from the asymmetry of the half–integer order carpet beams. These phase anomalies may guarantee an invariant intensity distribution during propagation. The phase is still symmetrical for two types of carpet beams.

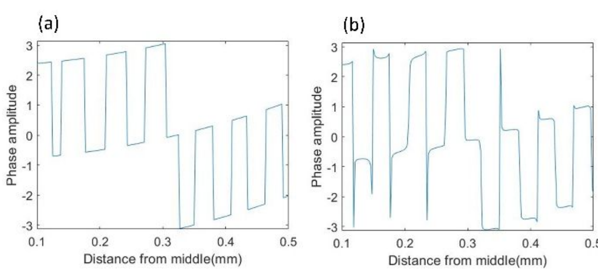

Fig. 3 Phase anomalies of the carpet beams. The phase profiles along the x axis with (a) q = 8; (b) q = 8.5.

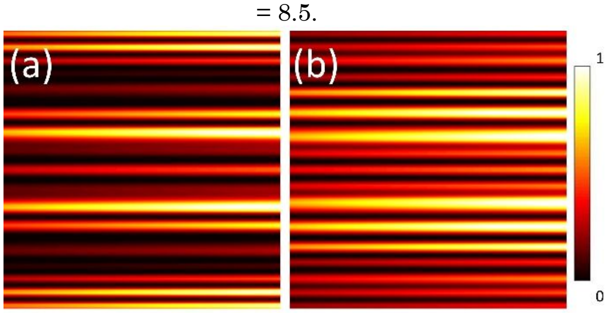

Fig. 4 x–z cross–section through the intensity volume carpet beams propagation. The location is taken from the white line in Fig. 2; (a) q=8; (b) q=8.5.

We also investigate the propagation characteristics of the two types of carpet beams. Without loss of generality, we arbitrary selected a cross–section diagram at a position of a beam. The theoretically simulated cross–sectional propagation graph is shown in Fig. 4. Each lattice of the carpet beams is non–diffracting during propagation. However, in the non–diffractive propagating distance, the optical intensity slightly increases for each lattice.

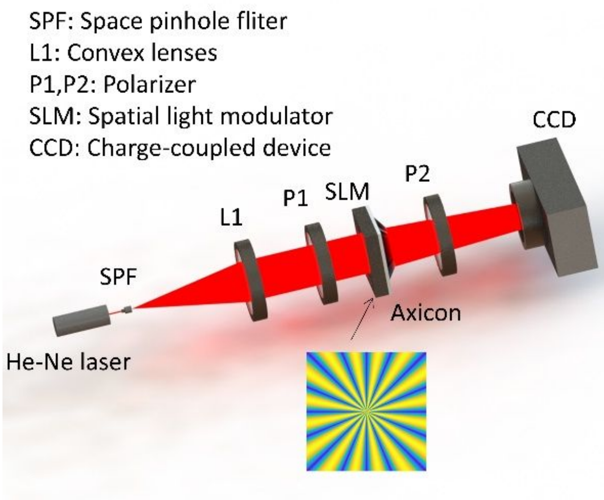

Fig. 5. Experimental system of generating carpet beams.

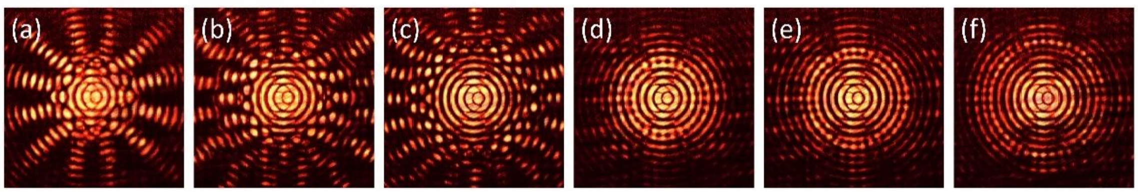

Fig. 6 Experimentally recorded graph of the integer order and half–order carpet beams with different spokes and the same parameters corresponding to Fig. 2.

The experimental setup of generating carpet beams is illustrated in Fig. 5. After He–Ne laser expansion and collimation (the wavelength is 632.8nm, and the radius of the expanded beam is approximately 4 cm), the plane wave illuminated the ETASR grating, which was tightly attached to the axicon. The base angle of the axicon is 1°, the entrance pupil radius of the axicon is 1.25 cm and refractive index is 1.457. The centers of the two elements were strictly aligned. The masks of the ETASR gratings were imposed on an amplitude–type spatial light modulator (SLM). These masks were loaded on the SLM one by one, and hence different carpet beams were generated. To improve the quality of the generated carpet beams, we added two polarizers before the grating and after the axicon. An optimal carpet beam was obtained after the polarizer was rotated. After the axicon, the modulated beam was Fresnel diffracted. Thus, the obtained beams were captured by using a high–resolution CCD camera (Fig. 6). According to the parameters of the axicon, the maximum non–diffraction distance of carpet beams was 1083 mm. According to Eq. (18), one can know that the shape of the beam is independent of the wavelength. It means that lasers in other wavelengths that can be modulated by SLM can also be used to generate the kind of non–diffracting carpet beams.

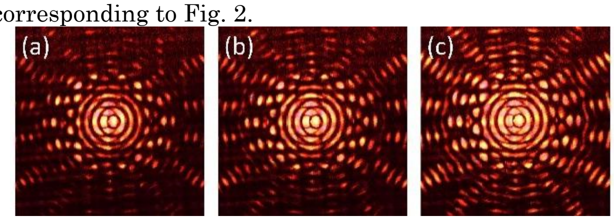

Fig. 7 Experimental recorded graph of 8-order carpet beams at different propagation distances after axicon. (a) z=70 cm; (b) z=80 cm; (c) z=90 cm.

The carpet beams were recorded at 80 cm after the axicon (Fig. 6). The recorded experimental diffraction patterns of ETASR grating with different parameters were in agreement with the theoretical simulated carpet beams. The introduced ETASR gratings were used to generate the novel carpet beams.

To verify the non–diffracting transmission characteristics of the generated carpet beams in the range of $z<z_{\max}$, we recorded the intensity distribution of 8–order carpet beams in the different propagation distances after the axicon (Fig. 7). The shapes of the optical structure of the carpet beams were almost preserved during propagation, although the light intensity slightly increased. Hence the generated caustic beams on the basis of the stationary phase principle can be regarded as non–diffracting beams.

4. Summary

We constructed novel non–diffracting carpet beams by introducing ETASR gratings. As a proof of concept, a theoretical derivation of this kind of carpet beams was first presented according to the principle of stationary phase. Then, by using an axicon and the

ETASR gratings, non–diffracting integer order and half–integer order carpet beams were generated. Their distinctive optical characteristics and phase anomalies of the integer order and half–integer order carpet beams were investigated for different cases. The generated non–diffracting carpet beams with the propagation–invariant divergent ring lattice structures and an extended depth of multiple focuses may open numerous potential applications for optical manipulation, optical processing, lattice light–sheet microscopy, and even other related applications.

References

[1] S. Rasouli, D. Hebri, A. M. Khazaei, "**Investigation of various behaviors of near–and far–field diffractions from multiplicatively separable structures in the x and y directions, and a detailed study of the near–field diffraction patterns of 2D multiplicatively separable periodic structures using the contrast variation method**", J Opt 2017;19(9):095601.

[2] K. Zhan, L. Dou, R. Jiao, W. Zhang, and B. Liu, "**Talbot effect in arrays of helical waveguides**", Opt. Lett. 46, 322–325 (2021)

[3] J. Zhao, Y. Wu, Z. Lin, D. Xu, H. Huang, C. Xu, Z. Tu, H. Liu, L. Shui, and D. Deng, "**Autofocusing self–imaging: symmetric Pearcey Talbot–like effect**", Opt. Express 30, 14146–14160 (2022)

[4] S. Rasouli, A. M. Khazaei, and D. Hebri, "**Radial carpet beams: A class of nondiffracting, accelerating, and self–healing beams**", Phys. Rev. A 97, 033844–Published 23 March 2018

[5] S. Rasouli, S. Hamzeloui, D. Hebri, "**Colorful radial Talbot carpet at the transverse plane**", Opt Express. 2019 Jun 24;27(13):17435–17448. doi: 10.1364/OE.27.017435. PMID: 31252703.

[6] S. Rasouli, A. M. Khazaei, and D. Hebri, "**Talbot carpet at the transverse plane produced in the diffraction of plane wave from amplitude radial gratings**", J. Opt. Soc. Am. A 35, 55–64 (2018)

[7] M. K. Karahroudi, M. K. Karahroudi, A. Mobashery, and B. Parmoon, "**Information transmission using radial carpet beams**", Appl. Opt. 58, 1886–1894 (2019)

[8] M. S. Kim, T. Scharf, C. Menzel, C. Rockstuhl, H. P. Herzig, "**Phase anomalies in Talbot light carpets of self–images**", Opt Express. 2013 Jan 14;21(1):1287–300. doi: 10.1364/OE.21.001287. PMID: 23389022.

[9] R. Azizkhani, D. Hebri, S. Rasouli, "**Gaussian beam diffraction from radial structures: detailed study on the diffraction from sinusoidal amplitude radial gratings**", Opt Express. 2023 Jun 19;31(13):20665–20682. doi: 10.1364/OE.489659. PMID: 37381185.

[10] J. Bayat, F. Hajizadeh, A. M. Khazaei, and S. Rasouli, "**Gear–like rotatable optical trapping with radial carpet beams**", Sci Rep 10, 11721 (2020).

[11] D. Hebri, S. Rasouli and M. Yeganeh, "**Intensity–based measuring of the topological charge alteration by the diffraction of vortex beams from amplitude sinusoidal radial gratings**", J. Opt. Soc. Am. B35, 724–730 (2018).

[12] M. K. Karahroudi and M. R. JafarFard, "**Detection and classification of radial carpet beams propagating through an underwater medium**", J. Opt. Soc. Am. B 40, 3006–3014 (2023)

[13] J. Durnin, J. J. Miceli Jr, J. H. Eberly, "**Diffraction–free beams**", Phys Rev Lett 1987;58 (15):1499–501.

[14] V. Garces–Chavez, D. McGloin, H. Melville, W. Sibbett, K. Dholakia, "**Simultaneous micromanipulation in multiple planes using a self–reconstructing light beam**", Nature 419 (2002) 145–147

[15] E. Betzig, G. H. Patterson, R. Sougrat, O. W. Lindwasser, S. Olenych, J. S. Bonifacino, M. W. Davidson, J. Lippincott–Schwartz, H. F. Hess, "**Imaging intracellular fluorescent proteins at nanometer resolution**", Science 313 (2006) 1642–1645

[16] P. J. Keller, A. D. Schmidt, A. Santella, K. Khairy, Z. Bao, J. Wittbrodt, E. H. K. Stelzer, "**Fast, high–contrast imaging of animal development with scanned light sheet–based structured–illumination microscopy**", Nature Methods 7 (2010) 637–642

[17] J. Wang, J. Yang, I. M. Fazal, N. Ahmed, Y. Yan, H. Huang, Y. Ren, Y. Yue, S. Dolinar, M. Tur, A. E. Willner, "**Terabit free–space data transmission employing orbital angular momentum multiplexing**" Nature Photon 6, 488–496 (2012).

[18] J. Baumgartl, M. Mazilu, K. Dholakia, "**Optically mediated particle clearing using Airy wavepackets**", Nat. Photon., 2(11): 675–678 (2008)

[19] M. Zhang, Z. Ren, and P. Yu, "**Improve depth of field of optical coherence tomography using finite energy Airy beam**", Opt. Lett. 44, 3158–3161 (2019)

[20] P. Polynkin, M. Kolesik, J. V. Moloney, G. A. Siviloglou, D. N. Christodoulides, "**Curved plasma channel generation using ultraintense Airy beams**", Science, 324: 229–232 (2009)

[21] L. Yu, Y. Zhang, "**Analysis of modal crosstalk for communication in turbulent ocean using Lommel–Gaussian beam**", Opt Express. 2017 Sep 18;25(19):22565–22574. doi: 10.1364/OE.25.022565. PMID: 29041564.

[22] A. Ortiz–Ambriz, J. C. Gutiérrez–Vega, and D. Petrov, "**Manipulation of dielectric particles with nondiffracting parabolic beams**", J. Opt. Soc. Am. A 31, 2759–2762 (2014)

[23] P. Rose, M. Boguslawski, and C. Denz, "**Nonlinear lattice structures based on families of complex nondiffracting beams**", New J. Phys. 14, 3 (2012).

[24] D. A. Ikonnikov, S. A. Myslivets, V. Arkhipkin, A. M. Vyunishev, "**3D Optical Vortex Lattices**", May 2021Annalen der Physik 533(7):2100114 DOI: 10.1002/andp.202100114

[25] S. López–Aguayo, Y. V. Kartashov, V. A. Vysloukh, and L. Torner, "**Method to Generate Complex Quasinondiffracting Optical Lattices**", Phys. Rev. Lett. 105, 013902 – Published 28 June 2010.

[26] R. Chen, Y. Shi, N. Gong, Y. Liu, and R. Ren, "**Generation of shaping nondiffracting structured caustic beams on the basis of stationary phase principle**", Chin. Opt. Lett. 21, 102601– (2023).

[27] S. Franke–Arnold, J. Leach, M. J. Padgett, V. E. Lembessis, D. Ellinas, A. J. Wright, J. M. Girkin, P. Öhberg, and A. S. Arnold, "**Optical ferris wheel for ultracold atoms**", Opt. Express 15(14), 8619–8625 (2007).

[28] A. Mathis, F. Courvoisier, L. Froehly, L. Furfaro, M. Jacquot, P. Lacourt, and J. Dudley, "**Micromachining

along a curve: Femtosecond laser micromachining of curved profiles in diamond and silicon using accelerating beams", Appl. Phys. Lett. 101, 071110 (2012).

[29] N. Gong, F. Xu, J. Yang, Y. Shi, Y. Qian, Z. Ren, "Generation of diffraction–free petallike beams based on stationary phase principle", Results in Physics, Volume 39,2022,105698,ISSN 2211–3797.

[30] N. Gong, J. Yang, Y. Ding, Y. Shi, R. Chen, Z. Ren, "Generation of Diffraction–Free Carpet Beams Based on Stationary Phase Method[J]", Acta Optica Sinica, 2022, 42(16): 1605001.

[31] J. H. McLeod, "The axicon: a new type of optical element", J Opt Soc Am 1954;44(8): 592–7.

[32] G. B. Arfken, H. J. Weber, and F. Harris, Mathematical Methods for Physicists (Academic, 2000).

[33] J. J. Stamnes, Waves in Focal Regions: Propagation, Diffraction and Focusing of Light, Sound and Water Waves (Taylor & Francis Group, 1986).

[34] L. G. Gouy, "Surune propriété nouvelle des ondes lumineuses", C. R. Acad. Sci. 110, 1251–1253 (1890).

[35] S. Feng and H. G. Winful, "Physical origin of the Gouy phase shift", Opt. Lett. 26, 485–487 (2001)

Acknowledgement

Funding. National Natural Science Foundation of China (11974314, 11674288).

Disclosures. The authors declare no conflicts of interest.

Data availability. Data underlying the results presented in this paper are not publicly available at the time but may be obtained from the author upon reasonable request.